

## Aging of Rubrene Layers in Ni/Rubrene Heterostructures Studied by Magneto-Optical Kerr Effect Spectroscopy

Wen Li, Michael Fronk, Hartmut Kupfer, Steffen Schulze, Michael Hietschold, Dietrich R. T. Zahn, and Georgeta Salvan\*

*Institute of Physics, Chemnitz University of Technology, D-09107 Chemnitz, Germany*

Received September 11, 2009; E-mail: salvan@physik.tu-chemnitz.de

**Abstract:** Magneto-optical Kerr effect (MOKE) spectroscopy was applied to probe the aging of Ni/rubrene bilayers under ambient atmosphere. A comparison between the simulated MOKE spectra of the heterostructure and the experimental MOKE spectra recorded at several time intervals after the samples were exposed to the ambient atmosphere demonstrates that the organic layer undergoes slow oxidation. The Ni top layer was found to exhibit capping properties, reducing the rate of oxidation of the organic underlayer in comparison with single organic layers.

### Introduction

Metal/organic heterostructures formed by the deposition of metals on organic films find a wide range of applications in organic electronics and spintronics.<sup>1–3</sup> The aging of devices containing organic materials has become an important research topic during the past few years (e.g., see ref 4).

In this work, we demonstrate that magneto-optical Kerr effect (MOKE) spectroscopy in the visible and UV spectral ranges can be applied to study the aging of heterostructures composed of magnetic metallic layers and organic layers under ambient atmosphere. As a model system, we used Ni/rubrene bilayers produced by successive deposition of the organic and metal layers in vacuum.

Rubrene (C<sub>42</sub>H<sub>28</sub>) is an organic semiconductor material often used in organic electronic or spintronic devices because of its high charge-carrier mobility<sup>5</sup> and long spin relaxation times.<sup>6</sup> When exposed to air, rubrene films oxidize to form rubrene peroxide,<sup>7</sup> which changes their optical properties.<sup>8</sup> The Lewis formulas of rubrene and rubrene peroxide are shown in Figure S1 in the Supporting Information. This behavior was exploited to prove the high sensitivity of MOKE spectroscopy with respect to the optical and chemical properties of Ni/rubrene structures. Since rubrene itself, like many other nonplanar molecules, has a negligible MOKE signal, the MOKE investigations required the presence of a ferromagnetic layer below or above the organic

layer. In this work, the configuration with the top metal layer, using the example of Ni, was considered because of its relevance for vertically stacked spintronic devices (e.g., see refs 3, 6, and 9).

### Experimental Section

In order to prepare Ni/rubrene bilayers, *p*-Si(111) substrates covered with 2.5 nm of native oxide were transferred into a high-vacuum chamber [(9 ± 3) × 10<sup>-9</sup> mbar] after being cleaned sequentially using acetone, ethanol, and deionized water in an ultrasonic bath for 5 min each. The rubrene source material was purified by gradient sublimation. The rubrene molecules were deposited onto the Si substrates by organic molecular beam deposition from a Knudsen cell at a rate of 0.11 ± 0.01 nm/min. Immediately after the deposition of rubrene, Ni was deposited onto the rubrene layer at a constant deposition rate of 0.26 ± 0.03 nm/min using an electron beam evaporator.

The magneto-optical measurements were performed *ex situ* using a homemade MOKE setup built according to ref 10 that allows spectroscopic measurements in the polar geometry at 0.35 T to be performed. The MOKE setup also allows the recording of the Kerr rotation angle as a function of applied magnetic field strength at a given energy, and thus, the magnetic hysteresis of the heterostructures can be recorded.

Atomic force microscopy (AFM) measurements were recorded using an AFM Autoprobe CP apparatus (Park Scientific Instruments). The images were acquired using sharpened microtips (MSCT-AUHW) in contact mode. All of the AFM pictures were flattened, and the sample tilt was removed by subtracting a second-order polynomial to eliminate scanner influences.

Transmission electron microscopy (TEM) investigations were performed using a Philips CM 20 FEG electron microscope.

### Results and Discussion

Figure 1 shows AFM images of two Ni/rubrene bilayers having different thicknesses of the rubrene underlayer. The bilayer Ni(14 nm)/rubrene(50 nm) (Figure 1a) covers the

- (1) *Organic Electronics: Materials, Manufacturing, and Applications*; Klauk, H., Ed.; Wiley-VCH: Weinheim, Germany, 2006.
- (2) Zahn, D. R. T.; Gavrila, G. N.; Salvan, G. *Chem. Rev.* **2007**, *107*, 1161.
- (3) Naber, W. J. M.; Faez, S.; van der Wiel, W. G. *J. Phys. D: Appl. Phys.* **2007**, *40*, R205.
- (4) Lehmann, D.; Zahn, D. R. T. *Appl. Phys. A: Mater. Sci. Process.* **2009**, *95*, 203.
- (5) Sundar, V. C.; Zaumseil, J.; Podzorov, V.; Menard, E.; Willett, R. L.; Someya, T.; Gershenson, M. E.; Rogers, J. A. *Science* **2004**, *303*, 1644.
- (6) Dediu, V. A.; Hueso, L. E.; Bergenti, I.; Taliani, C. *Nat. Mater.* **2009**, *8*, 707.
- (7) Kloc, C.; Tan, K. J.; Toh, M. L.; Zhang, K. K.; Xu, Y. P. *Appl. Phys. A: Mater. Sci. Process.* **2009**, *95*, 219.
- (8) Kytka, M.; Gerlach, A.; Schreiber, F.; Kovác, J. *Appl. Phys. Lett.* **2007**, *90*, 131911.

- (9) Xiong, Z. H.; Wu, D.; Vardeny, Z. V.; Shi, J. *Nature* **2004**, *427*, 821.
- (10) Herrmann, Th.; Lüdge, K.; Richter, W.; Georgarakis, K. G.; Pouloupoulos, P.; Nünthel, R.; Lindner, J.; Wahl, M.; Esser, N. *Phys. Rev. B* **2006**, *73*, 134408.

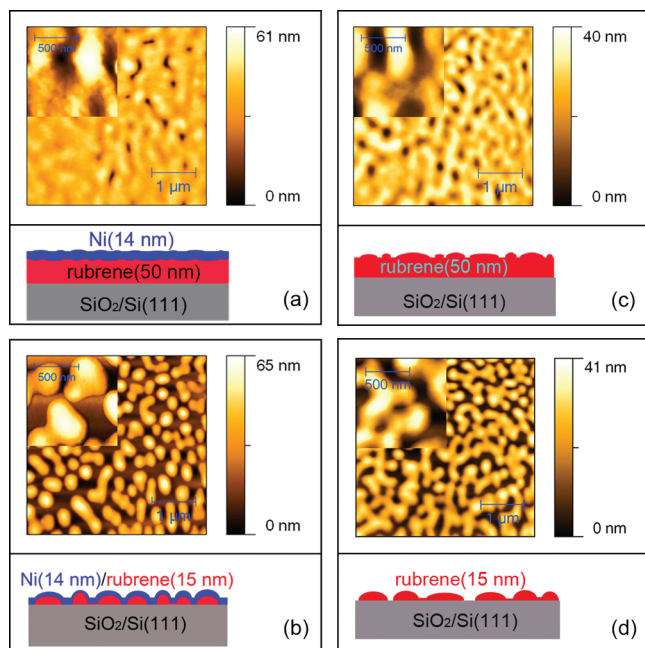


**Figure 1.** AFM images of (a) Ni(14 nm)/rubrene(50 nm) and (b) Ni(14 nm)/rubrene(15 nm) bilayers. For comparison, AFM images of rubrene single layers having thicknesses of 50 and 15 nm are shown in (c) and (d), respectively. The insets are  $1 \mu\text{m} \times 1 \mu\text{m}$  scan AFM images that have been enlarged by a factor of 2. The sketches at the bottom present schematically the structures of the corresponding samples.

substrate almost homogeneously with only a few voids. The inset shows that the surface of this bilayer exhibits a fine structure with lateral dimensions of  $\sim 50$  nm. The AFM images of the Ni(14 nm)/rubrene(15 nm) bilayer show well-separated islands with a lateral size of 100–200 nm (Figure 1b).

AFM images of single rubrene layers having the same thicknesses as in the heterostructures (Figure 1c,d) reveal great similarities between the morphologies of the single rubrene layers and those of the corresponding heterostructures. However, the heterostructures exhibit a granular substructure with lateral dimensions of 30–50 nm that is superimposed on the rubrene-like morphology (see the insets in Figure 1a,b as well as Figure S2 in the Supporting Information) and could be ascribed to the covering Ni film. This leads to the hypothesis that the islands should be formed by rubrene and are later covered by Ni.

To elucidate the structure of the bilayers, additional TEM investigations were performed. Since the bilayers were grown on a Si substrate, the following sample preparation was used for removing the films from the substrate: a film of amorphous carbon was first deposited onto the samples. Subsequently, the samples were inserted into acetone, and a Cu hole mask was pressed onto the amorphous C film. In the case of the Ni(14 nm)/rubrene(50 nm) sample, this procedure led to easy removal of the C film with the Ni layer sticking on it, while in the case of the Ni(14 nm)/rubrene(15 nm), only a few regions of the C film with very little Ni sticking to it could be removed. In Figure 2, the dark regions in the TEM images correspond to Ni and the bright regions to C. The presence of nanocrystalline Ni on the C film was proven in both cases by complementary electron diffraction measurements (see Figure S3 in the Supporting Information). A comparison of the TEM images (Figure 2) with the AFM images of the samples (Figure 1) shows that the C film perfectly copies the morphology of the corresponding sample.

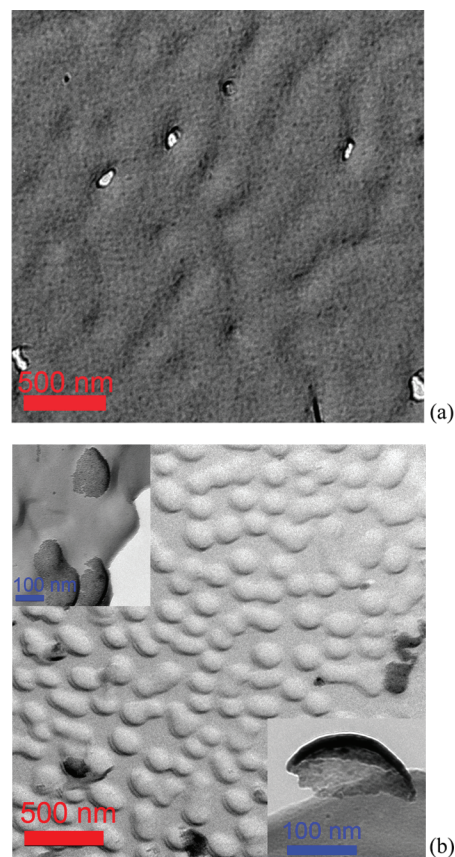


**Figure 2.** TEM images of Ni-covered carbon films detached from (a) Ni(14 nm)/rubrene(50 nm) and (b) Ni(14 nm)/rubrene(15 nm). The insets in (b) show higher-magnification sections that include dark patches representing pieces of the Ni caps.

The presence of only few Ni regions in Figure 2b can be understood if one considers the following scenario: The thin (15 nm) rubrene film grows in islands because of its relatively high mobility<sup>11</sup> on the substrate at the low evaporation rate used in our experiment. Ni follows the morphology of the rubrene islands, capping them and filling the space between the islands. The granular structure of the bilayer probably hinders acetone from completely dissolving the Ni-capped rubrene islands. However, some of the Ni regions that could be detached from the sample exhibit a caplike shape (see the lower inset in Figure 2b), providing clear evidence for the fact that the islands observed in the AFM images consist of rubrene and are capped by Ni.

The continuous Ni coverage of the C film in Figure 2a can be explained considering that a continuous Ni film is formed on the thicker and smoother 50 nm rubrene layer. The rubrene layer is most probably entirely dissolved by acetone during the sample preparation for TEM, and the Ni film originally formed on top of it can easily be removed together with the C film. This is an indication that under the evaporation conditions used in this work, a thickness of 50 nm is enough for the rubrene islands to merge and form an almost closed layer.

The magnetic hysteresis curves of the Ni/rubrene heterostructures were measured by MOKE spectroscopy at 3.5 eV in the polar geometry at room temperature and exhibit a combination of superparamagnetic and ferromagnetic behavior, with the easy axis in the plane of the Ni film.<sup>12</sup>

(11) Ribière, P. R.; Bratina, G. *Surf. Sci.* **2008**, *602*, 1368.

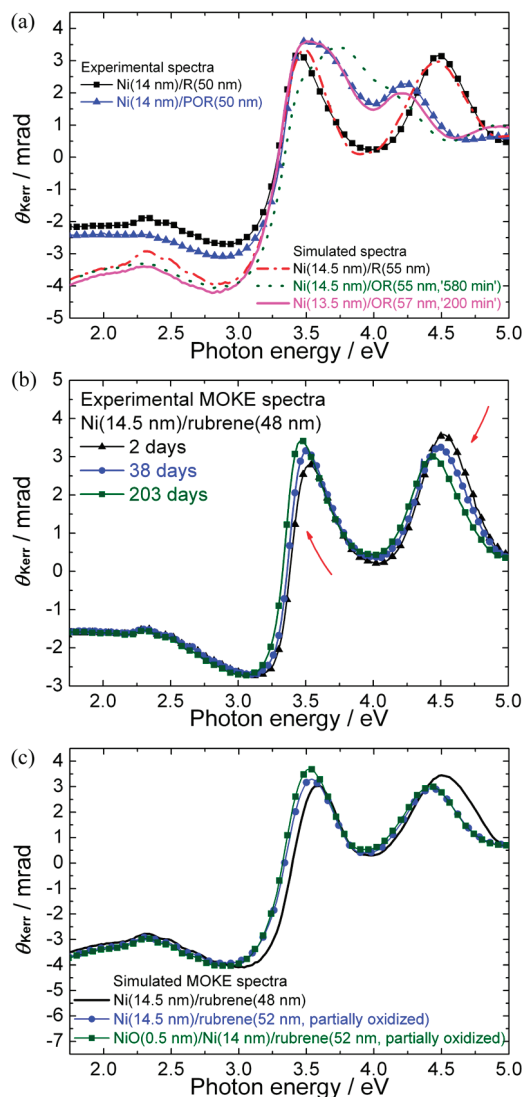


**Figure 3.** (a) Experimental and simulated MOKE spectra of Ni(14 nm)/rubrene(50 nm) bilayers. The abbreviations R, OR, and POR stand for pristine rubrene, photo-oxidized rubrene, and preoxidized rubrene, respectively. (b) Experimental MOKE spectra of a Ni(14 nm)/rubrene(50 nm) bilayer recorded at several times after removal from UHV. (c) Simulated MOKE spectra for Ni(14 nm)/rubrene bilayers using the optical constants of a rubrene layer exposed for 870 min at an air pressure of 40 mbar (taken from ref 8).

All of the MOKE spectra were recorded in saturation (at 0.35 T) in order to exclude the effect of variations in the magnetic properties on the following simulations.

Figure 3a shows experimental MOKE spectra of 14 nm Ni layers deposited onto 50 nm layers of pristine rubrene (line plus squares) and preoxidized rubrene (see below) (line plus triangles). Both of the experimental spectra in Figure 3a were recorded immediately after the samples were exposed to air. The recording of a MOKE spectrum took  $\sim 400$  min. In the following, we will refer to the rubrene (R) underlayer when the Ni layer was grown onto freshly prepared pristine rubrene layers or to the preoxidized rubrene (POR) underlayer when the rubrene layer was exposed to the ambient atmosphere for 60 min prior to Ni deposition. In some cases, the optical

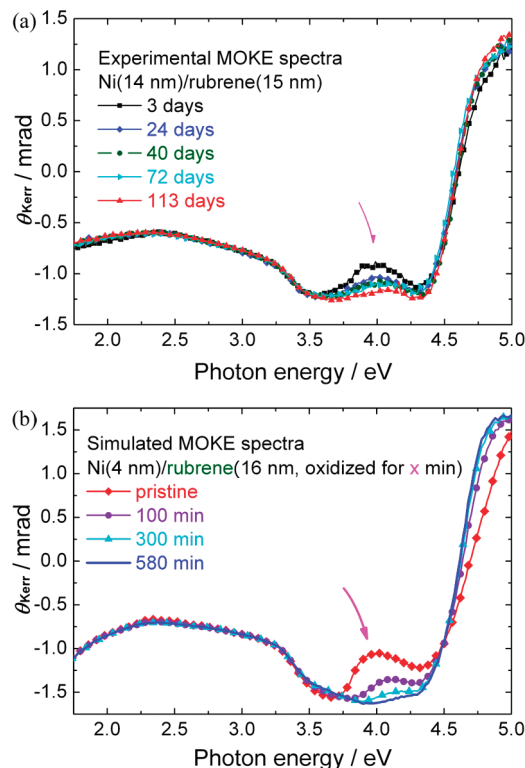


**Figure 4.** (a) MOKE spectra of a Ni(14 nm)/rubrene(15 nm) bilayer recorded upon aging in air. (b) Simulated MOKE spectra of a Ni(4 nm)/rubrene(16 nm) bilayer performed using the optical constants of a rubrene layer that was photo-oxidized<sup>8</sup> for the time intervals shown in the legend.

constants of oxidized rubrene (OR) obtained by exposing a rubrene layer to air under Xe lamp illumination for different time intervals (taken from ref 8) were considered in the simulations.

Because of its low thickness (14 nm), the Ni layer is transparent to light over the measured spectral range. The light transmitted through the Ni layer is reflected multiple times at the rubrene/substrate and rubrene/Ni interfaces. The interference of the light beams leaving the sample has significant influence on the MOKE spectra: depending on the thickness of the rubrene layer, the spectral features can undergo energetic shifts, changes in magnitude, or even changes in sign (compare Figures 3a and 4a). In order to simulate the MOKE spectra, we used an extension of the model presented in a previous paper<sup>13</sup> (see Simulation Model, below). Here, two layers were inserted between air and the substrate, and in some cases even more layers were considered (e.g., to account for NiO). In the simulations, the optical constants of each layer<sup>8,14</sup> and the Voigt constant of the magnetic layer<sup>10</sup> were entered as input parameters. The details of the simulation are explained in Simulation Model.

The MOKE spectrum simulated using the optical constants<sup>8</sup> of pristine rubrene (dash-dotted line in Figure 4a) fit the corresponding experimental spectrum very well, especially in the spectral range from 3.2 to 5 eV. Also, the doublet spectral feature at 2.3 and 2.5 eV, which stems from the optical absorption of the energetically lowest transitions of rubrene,

(13) Fronk, M.; Bräuer, B.; Kortus, J.; Schmidt, O. G.; Zahn, D. R. T.; Salvan, G. *Phys. Rev. B* **2009**, *79*, 235305.

(14) *Handbook of Optical Constants of Solids*; Palik, E. D., Ed; Academic Press: New York, 1985.

(12) Li, W.; Fronk, M.; Kupfer, H.; Springer, F.; Liebig, A.; Albrecht, M.; Zahn, D. R. T.; Salvan, G. In preparation.

was well-reproduced. It should be noted that all of the simulated MOKE spectra showed a similar offset with respect to the experimental spectra in the range from 1.75 to 3 eV, which may be caused by a difference between the optical constants of the Ni bulk and those of the thin Ni films, a difference between the Voigt constant of a freshly prepared smooth Ni film that was not exposed to atmosphere (taken from ref 10) and that of the Ni film in our heterostructure, and/or depolarization effects related to the roughness of the samples. When the optical constants of OR, which was photo-oxidized for 580 min,<sup>8</sup> were used in the simulation, the calculated MOKE spectrum (Figure 3a, dotted line) deviated significantly from the experimental spectrum between 3.5 and 5 eV. The effective thicknesses of Ni and rubrene considered in the simulations were  $14.5 \pm 0.5$  and  $55 \pm 1$  nm, respectively, which are very close to the nominal thicknesses (14 and 50 nm, respectively) determined experimentally from the Ni flux of the electron beam evaporator and the frequency shift of a quartz microbalance, respectively. It must be noted that MOKE simulations considering organic layers having optical constants different from those of the pristine rubrene did not improve the match between the calculated spectrum and the spectrum of the heterostructure prepared with the pristine layer.

In order to experimentally confirm the influence of the optical constants of the organic layer on the shape of the MOKE spectra, a 50 nm rubrene layer was exposed to air for 60 min to obtain the POR layer before the deposition of a 14 nm Ni layer onto it. According to refs 7, 8, and 15, this should be sufficient to at least partially oxidize the rubrene layer. The MOKE spectrum of this sample (Figure 3a, line plus triangles) shows two significant changes compared with that of the Ni(14 nm)/pristine rubrene(50 nm) sample: the doublet feature at 2.3 and 2.5 eV has disappeared, and the second main feature has shifted from 4.5 to 4.2 eV with a decrease in amplitude. When the MOKE spectrum of this sample was simulated, a structure consisting of a  $13.5 \pm 0.5$  nm Ni layer on a  $57 \pm 1$  nm organic layer having the optical constants of rubrene photo-oxidized for 200 min,<sup>8</sup> was found to fit the experimental spectrum best. The excellent agreement between the simulated and experimental spectra indicates that the exposure of a 50 nm rubrene layer for 60 min to air resulted in the partial oxidation of the rubrene layer.

Since the measurement of one MOKE spectrum took ~400 min in atmosphere, the very good match between the simulated and experimental spectra in both cases presented above provides a strong hint that the Ni layer acts as a capping layer. In addition, the good match between the Ni thickness used in the simulations and the experimental nominal thickness shows that the Ni film itself does not undergo strong oxidation.

In order to check the capping efficiency of the Ni top layer, MOKE spectra of a Ni(14.5 nm)/pristine rubrene(48 nm) sample were recorded at several times after exposure to air (Figure 3b). The shape of the MOKE spectrum changed slightly with exposure time. The same trends as in the case of Ni/POR (i.e., a red shift, an increase in intensity of the feature at ~3.4 eV, and a decrease in intensity of the feature at ~4.5 eV, albeit less pronounced) were observed. These slight spectral changes indicate that the organic underlayer oxidizes in air very slowly, on a time scale of months.

MOKE simulations showed that while the red shift of the feature at ~4.5 eV could be reproduced using rubrene oxidized

for 870 min at 40 mbar air pressure at a thickness equal to that of the pristine rubrene (48 nm), the red shift of the feature at ~3.4 eV with the time of aging could only be explained if the oxidation of the rubrene underlayer was considered to be accompanied by an increase in the thickness of the rubrene film (Figure 3c, line plus circles). The increase in thickness upon oxidation was reported previously.<sup>8</sup> On the other hand, the magnitude of the amplitude increase of the feature at ~3.4 eV could not be reproduced in simulations by changing either the optical constants or the thickness of the rubrene layer, but the behavior could be simulated by considering the formation of a thin NiO layer ( $0.5 \pm 0.2$  nm) on top of the Ni layer (Figure 3c, line plus squares). This demonstrates the sensitivity of MOKE spectroscopy to parameter changes in both the metal and the organic underlayer.

In the MOKE spectrum of the Ni(14 nm)/rubrene(15 nm) bilayer (Figure 4a), the main spectral features have a negative sign, in contrast to the case of Ni(14 nm)/rubrene(50 nm) and a spectral shape similar to single Ni layer.<sup>10</sup> It should be noted that the samples investigated in this work that had a low thickness of the rubrene underlayer (12–15 nm) exhibited only slight differences in their MOKE spectra recorded soon after exposure to atmosphere, and their morphology probed by AFM displayed no noticeable differences. However, they showed a large spread in the rate of oxidation of the rubrene underlayer, depending, for example, on the base pressure or waiting time between the deposition of rubrene and Ni. For the following discussion, we have chosen the sample with the highest rubrene oxidation rate.

The doublet feature near 2.6 and 2.8 eV related to the optical absorption in rubrene was not observed. The evolution of the MOKE spectrum of the Ni(14 nm)/rubrene(15 nm) bilayer with the air exposure time is also presented in Figure 4a. The main spectral change is the decrease in the feature at ~4 eV.

The application of the layered model in the simulations qualitatively reproduced the trends in the experimental MOKE spectra. For the best fit to the experimental MOKE spectrum, however, an effective thickness of Ni of only 4 nm, which is much smaller than the nominal thickness of 14 nm, had to be used in the simulations (Figure 4b), indicating that a more sophisticated optical model is needed to accurately describe the properties of the Ni layer. Using the optical constants of a mixed Ni/rubrene layer modeled by the effective medium approximation, a model expected to work for islands in the nanometer range, did not improve the simulation results. Further simulation work to clarify this issue is in progress.

Even though the layered optical model has to be considered with care, it was applied in the following to qualitatively estimate the effect of rubrene oxidation on the MOKE spectra using the optical constants reported by Kytka et al.<sup>8</sup> for a rubrene layer that was photo-oxidized by exposure to air under Xe lamp illumination for 100, 300, and 580 min. Comparison of the simulation results to the experimental spectra clearly shows that the spectral changes near 4 eV over time can be ascribed to the alteration of the optical constants of the rubrene underlayer due to its oxidation. It should be noted that during each MOKE measurement, the sample also was illuminated by a Xe lamp for ~400 min. From a comparison of the time scales in panels (a) and (b) of Figure 4, it becomes evident that although the Ni top layer does not prevent the oxidation of the rubrene underlayer, it certainly slows that process significantly. For example, the MOKE spectrum calculated with the optical constants of rubrene exposed to 40 mbar air and illuminated

(15) Käfer, D.; Witte, G. *Phys. Chem. Chem. Phys.* **2005**, *7*, 2850.

with a 75 W Xe lamp for 300 min is comparable to the experimental MOKE spectrum of the bilayer aged for 113 days and exposed five times to a 75 W Xe lamp for ~400 min each time. Thus, even when the bilayer consists of distinct large islands, the Ni top layer still shows a capping effect.

According to ref 8, oxidation and photo-oxidation affect the optical constants of rubrene in the same manner (decreasing the amplitude of the bands around 2.5 and 4 eV and increasing the intensity of the band around 4.75 eV), but the change is significantly faster upon photo-oxidation. While the optical constants<sup>8</sup> of rubrene oxidized for 870 min at 40 mbar air pressure without illumination reproduced well the experiment in the case of Ni(14 nm)/rubrene(50 nm), optical constants of rubrene exposed to photo-oxidation had to be taken into account to reproduce the MOKE spectra of Ni(14 nm)/rubrene(15 nm).

## Conclusions

Using the example of Ni/rubrene bilayers, we have demonstrated that MOKE spectroscopy is a powerful method for indirectly probing the optical and thereby the chemical properties of organic layers in ferromagnetic/organic bilayers, a configuration often met in organic spintronic devices. In addition, MOKE measurements at a fixed photon energy as a function of the applied magnetic field strength can deliver information about the magnetic properties of the metal layer.

The origin of the MOKE signal of the heterostructure lies in the change in the polarization state of the light caused by the Ni layer. A change in the rubrene layer thickness from 15 to 50 nm, however, was found to have a dramatic influence on the MOKE spectrum as a result of the interference of the light beams reflected at the Ni surface and those transmitted through the Ni layer and multiply reflected at the Ni/rubrene and rubrene/substrate interfaces. This provides the high sensitivity of the MOKE spectra to changes in the optical constants of the organic layer.

For both of the investigated morphology types of the Ni/rubrene heterostructure, Ni acted as a capping layer for the rubrene underlayer, significantly reducing the rate of oxidation upon exposure to the ambient atmosphere.

## Simulation Model

The change in the polarization state induced by reflection from a sample under a magnetic field is known as the magneto-optical Kerr effect.<sup>16,17</sup> This effect originates in the modification of the dielectric properties of the material in the presence of a magnetic field and can be described by a material parameter  $Q$ , the so-called Voigt constant.

In order to simulate the MOKE spectra of Ni/rubrene bilayers, we made the following assumptions:

1. As shown in Figure 5, the optical system has four components: the half-space air, a top layer with thickness  $d_T$ , a bottom layer with thickness  $d_B$ , and the substrate. The substrate is also treated as a half space because of its relatively large thickness in comparison with the penetration length of light over the measured spectral range.

2. The layers have spatially homogeneous optical constants. The optical constants of Si,<sup>18</sup> SiO<sub>2</sub>,<sup>14</sup> Ni,<sup>14</sup> NiO,<sup>19</sup> and rubrene<sup>8</sup> were taken from literature.

3. The interfaces are perfectly flat, and all of the reflections are considered using geometric series.

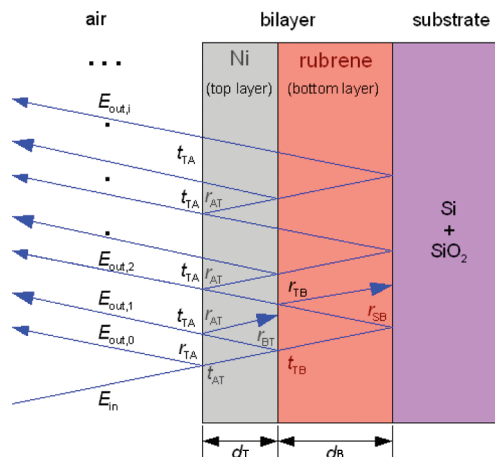


**Figure 5.** Illustration of the simulation model. The sketch holds for each of the two circular polarization states of the light, and the electric field vectors of the outgoing radiation,  $\mathbf{E}_{\text{out}}$ , are summed separately for each of the two circular polarization states. For better visualization, the angle of incidence is shown to be larger than zero in the sketch, although the model was constructed for the case of normal incidence.

4. The angle of incidence is zero.

5. The magnetism of every layer is neglected, except for the Ni layer, in which the optical constant  $\tilde{n}$  becomes different for different circular polarizations of light ( $\sigma^+$  and  $\sigma^-$ ) in a polar magnetic field:

$$\tilde{n}_{\pm} = \tilde{n} \left( 1 \mp \frac{Q}{2} \right) \quad (1)$$

The value of the Voigt constant  $Q$  for Ni used in eq 1 was taken from ref 10.

The lack of MOKE signals from the substrate and the single rubrene layer on the substrate was checked experimentally in this work.

The Fresnel formulas for the transmission ( $t$ ) and reflection ( $r$ ) coefficients along with the exponential phase/attenuation factors  $a$  on the paths inside the layers are used in order to calculate the effective reflection coefficient  $u$  for the top–bottom–substrate system:

$$u = \frac{r_{AT} + a_T^2 u_{TB}}{1 + a_T^2 u_{TB} r_{AT}} \quad (2)$$

in which

$$u_{TB} = \frac{r_{TB} + a_B^2 r_{BS}}{1 + a_B^2 r_{BS} r_{TB}} \quad (3)$$

where the labels A, T, B, and S stand for air, the top layer, the bottom layer, and the substrate (Si covered by 2.5 nm native SiO<sub>2</sub>), respectively. The quantities  $t_{JK}$ ,  $r_{JK}$ , and  $a_J$  (where J, K = A, T, B, S) are given by

$$t_{JK} = \frac{2\tilde{n}_J}{\tilde{n}_J + \tilde{n}_K} \quad (4)$$

$$r_{JK} = \frac{\tilde{n}_J - \tilde{n}_K}{\tilde{n}_J + \tilde{n}_K} \quad (5)$$

and

$$a_J = \exp \left[ i\tilde{n}_J \left( \frac{\omega}{c} \right) d_J \right] \quad (6)$$

(16) *Modern Magneto-optics and Magneto-optical Materials*; Zvezdin, A. K., Kotov, V. A., Eds.; IOP Publishing Ltd.: Philadelphia, 1997.

(17) *Magneto-Optics*; Sugano, S., Kojima, N., Eds.; Springer: Berlin, 2000.

(18) Jellison, G. E., Jr. *Opt. Mater.* **1992**, *1*, 41.

(19) Mendoza-Galván, A.; Vidales-Hurtado, M. A.; López-Beltrán, A. M. *Thin Solid Films* **2009**, *517*, 3115.

When the Jones formalism is used and the incident linearly polarized light is decomposed into the two circular components

$$J_+ = \frac{1}{2} \begin{pmatrix} 1 \\ i \end{pmatrix} \quad \text{and} \quad J_- = \frac{1}{2} \begin{pmatrix} 1 \\ -i \end{pmatrix} \quad (7)$$

which are the eigenmodes of the light in the given geometry and are modified separately by  $u_+$  and  $u_-$ , respectively, upon reflection from the sample, the complex Kerr angle can be calculated as

$$\Theta_K = \arctan \left[ i \frac{(u_+ - u_-)}{(u_+ + u_-)} \right] \quad (8)$$

On the basis of the above model, the MOKE spectra of Ni/rubrene bilayers were calculated using eq 8. The formulas were implemented in a Python script making use of the packages “NumPy” and “SciPy”.<sup>20</sup>

**Acknowledgment.** The authors thank M. Kytka for providing the optical constants of oxidized rubrene. The German Ministry for Education and Research and the German Science Foundation (Project FG 1154) are gratefully acknowledged for support.

**Supporting Information Available:** Lewis formulas of rubrene and rubrene peroxide (Figure S1), AFM images of rubrene single layers and Ni/rubrene bilayers (Figure S2), and electron diffraction images of Ni-covered carbon films detached from Ni/rubrene heterostructures (Figure S3). This material is available free of charge via the Internet at <http://pubs.acs.org>.

JA907728Y

---

(20) See: <http://scipy.org/>.